FLYWHEEL: JURNAL TEKNIK MESIN UNTIRTA

Homepagejurnal: http://jurnal.untirta.ac.id/index.php/jwl

Viscous Damping Coefficient Measurement System Using Incremental Optical Encoder

Arief Sudarmaji, Arifrahman Yustika Putra, Efta Yudiarsah*

Department of Physics, Universitas Indonesia, Depok 16424, Indonesia.

*Corresponding author: *e.yudiarsah@sci.ui.ac.id*

ARTICLE INFO

Received 26/03/2023
revision 05/04/2023
accepted 30/05/2023
Available online 01/06/2023

ABSTRACT

We built a viscous damping coefficient measurement system that applies the principles of underdamped harmonic oscillation within the viscous liquid. The scientific novelty of this paper lies in the type of sensor used to capture the oscillation. An incremental optical encoder is chosen as a motion detector due to its ability to convert angular position and rotation direction into a pair of square wave signals. The harmonic oscillator system consists of a spring with a constant value of 82.8 N/m, a 1.50 kg cylindrical mass, and a 95.0 g prolate ellipsoidal mass. The data acquisition system converts the encoder output pulses into counts, representing the oscillating mass displacements under the viscous liquid. We used a Proportional Integral Derivative (PID) temperature control system to maintain the sample temperature constant. Experimental data suggest that the mechanical components' air resistance and total friction contribute to the damping effect of the mass harmonic oscillation. ISO VG 100 oil sample is used to test the precision of the viscous damping coefficient system. The repeatability test of the ISO VG 100 damping coefficient measurement resulted in a 1.3% of relative standard deviation.

Keywords: *viscous damping coefficient, underdamped harmonic oscillation, encoder, temperature control system.*

1. INTRODUCTION

Innovation in technology has brought significant impacts on the automotive industry. Thus, the gap between the mechanical components of automotive engines gets narrower over time [1]. Unquestionably, lubricant oil plays a vital role in the modern world because it is needed to minimize friction between moving engine parts [2]. Viscosity is one of the most important physical properties regarding engine oil lubrication performance [3]. The *Society of Automotive Engineers* (SAE) and the *International Organization for Standardization* (ISO) have established the standard viscosity grades for engine and industrial oil products. In addition, viscosity is also one of the major parameters which determine the manufacturing process in the industry of liquid consumables [4].

In order to keep a product's viscosity value that agrees with the accepted standard value, liquid manufacturer companies use viscometers as their main quality control instruments [5]. Some of the most well-known types of viscometers are rotational viscometers, capillary viscometers, falling sphere viscometers, high-temperature viscometers, and ultrasonic viscometers [6]. All of these viscosity measurement devices work with different principles, and most of them are high-priced.

However, another principle that can also be used to measure liquid viscosity is the application of the Stokes drag formula. Stokes' law states that the drag force experienced by a spherical mass settling under viscous fluid (with dynamic viscosity) is proportional to the velocity of the mass, as reflected in Eq. 1 [7,8].

$$F_d = -c\mu v \quad (1)$$

Where is a constant that depends on the mass's shape and dimension? For a particular case where a mass oscillates through a fluid column, the retarding force obeys Eq. 2 [9].

$$F_d = -bv \quad (2)$$

Where is the viscous damping coefficient of the oscillatory motion? The formula of liquid dynamic viscosity can be obtained by substituting the right side of Eq. 1 to Eq. 2.

A few experimental types of research related to viscosity and damping coefficient measurements that rely on the underdamped oscillatory motion principles have been done. Alexander and Indelicato built an oscillator system that consists of a spherical mass attached to the lower end of a spring and used a force sensor to record the Stokes' drag against time [10]. Shamim, Zia, and Anwar built a similar spring-mass oscillator system setup using a webcam to capture the oscillatory motion [11]. Another design was proposed by Escalante-Martinez et al., where they reported using a simple viscously damped spring-mass system to measure the liquid damping coefficient [12]. They used a laser beam and a timer to measure the time it takes for the mass to reach two consecutive peaks during the underdamped oscillation.

This paper refers to a similar design of a spring-mass harmonic oscillator system that can be used to measure the viscous damping coefficient. Since an incremental optical encoder has yet to be used in previous studies, we decided to use it to capture the underdamped oscillatory motion of the spring-mass system. In addition, rotary encoders are suitable for the job because they can convert rotational movements into a pair of square wave signals with a 90° phase difference [13,14]. Unlike the previous studies, we added a PID-based temperature control system that heats the liquid container and maintains the sample's constant temperature. The sample temperature needs to be preserved because liquid viscosity varies with temperature [15].

2. METHODOLOGY

The oscillator system consists of a spring with a spring constant value of 82.8 N/m, a 1.50 kg cylindrical mass, and also a 95.0 g prolate ellipsoidal mass which stays within a cylindrical liquid container, as shown in Fig.1. It is added to the system to oppose the friction of the mechanical components which dominates the oscillation damping for low-viscosity liquid measurements, while experiences the Stokes drag which damps the oscillatory motion within the viscous liquid.

We chose a prolate ellipsoid as the shape of because for two reasons. First, it has smooth and narrowing surfaces on both ends. Thus, we expect to encounter a low possibility of turbulent flow since Stokes' law only applies in a low Reynolds number regime [16]. Second, Happel and Brenner have determined the appropriate Stokes drag model for a specific case where a prolate ellipsoid moves along its major axis through a liquid column [17].

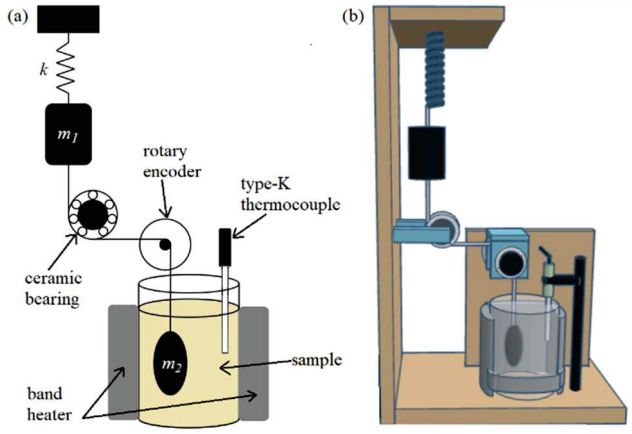

Figure 1. Experimental system setup: (a) Schematic diagram; (b) Three-Dimensional model.

The prolate ellipsoidal mass has a semi-major axis of 3.10 cm and a semi-minor axis of 0.815 cm. We used an LPD3806-600BM-G5-24C incremental optical encoder connected to a data acquisition system to encode the rotational movement of the shaft due to the underdamped oscillation. The encoder user's manual states that 600 square wave pulses are generated for every encoder shaft rotation. In addition, a ceramic ball bearing is also placed in the system's mechanical construction to allow the encoder shaft to rotate during the measurements.

2.1. Oscillation Data Acquisition System

An Arduino Nano V3.0 is chosen to be the microcontroller of the oscillation data acquisition system. The Arduino behaves as an *Up/Down* (U/D) counter, receiving a U/D input signal and generating counts based on *the clock* (CLK) pulses. During the underdamped harmonic oscillation, A D flip flop (from the 7474 IC) receives both pulses of the encoder output and generates the U/D signal [18]. Both encoder square wave outputs are also received by an XOR gate (from the 7486 IC) to generate the CLK signal, which has a frequency twice of the XOR

gate inputs [19]. Fig.2 shows the system block diagram.

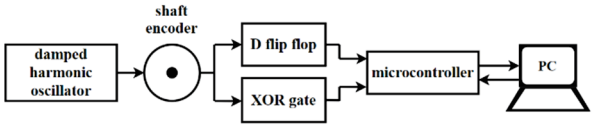

Figure 2. Data acquisition system block diagram.

The microcontroller generates the output of the U/D counter operation as integer counts and sends them to a LabVIEW program in the PC via Arduino Nano's serial communication protocol. The counts are converted into displacements according to the circumference of the encoder shaft. Once the underdamped oscillation against time is obtained, the damping coefficient can be calculated by generating the suitable exponential amplitude decay regression curve. Fig.3 shows the Printed Circuit Board (PCB) schematic diagram and the oscillation data acquisition system flow chart. It can be seen clearly in the diagram that we provided two different input channels for the encoder output signals (CA and CB). The user can choose either one of those channels as the data acquisition system route.

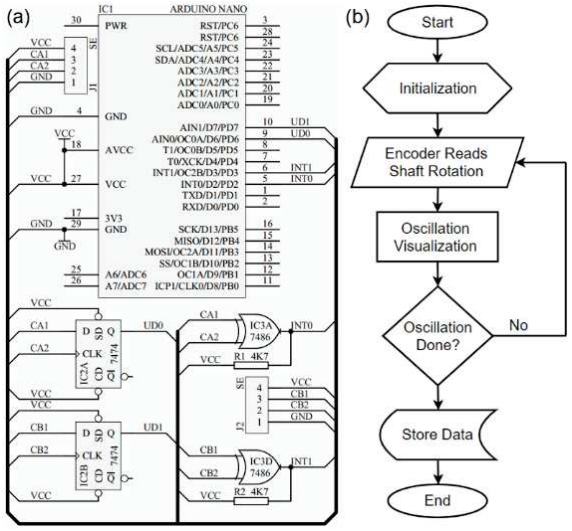

Figure 3. Data acquisition system: (a) PCB Schematic diagram; (b) Flow chart.

2.2. Temperature Control System

The liquid sample tested in this research has its specification of viscosity value at a certain point of temperature [20]. In order to get an accurate measurement result, the damping coefficient measurement system needs a temperature controller to maintain the sample's temperature at the specified point. We decided to add a PID-based temperature control system which consists of a 250 W band heater that is attached to a cylindrical metal liquid container, a type-K thermocouple probe, a MAX6675 digital thermometer module, a *Solid-State Relay* (SSR)-40 DA module, another Arduino Nano V3.0 as the microcontroller and a 220 VAC voltage supply. The type-K thermocouple probe is used in a specified temperature measurement range of -50 to 750 °C. Since the experimental procedures include temperature measurements within the thermocouple-specified working range, it is safe to declare that the thermocouple selection is suitable for this research. The cylindrical container's height is 28 cm, and we want the sample fluid to be heated uniformly. In order to achieve that, we used a band heater that is 25 cm in height. Fig.4 shows the block diagram, while Fig.5 Shows the PCB schematic diagram of the PID temperature control system.

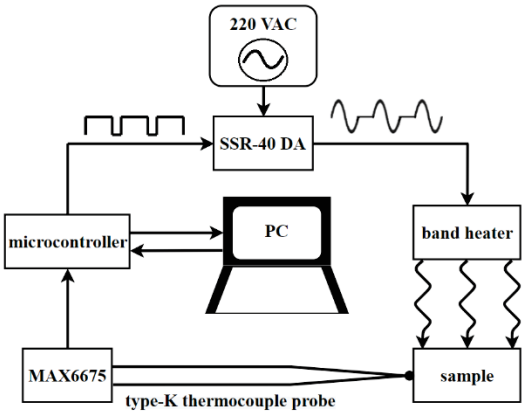

Figure 4. PID temperature control system block diagram.

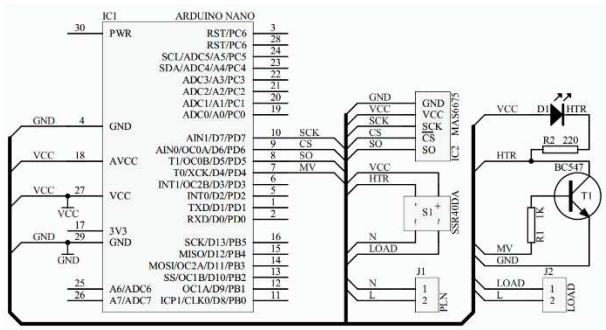

Figure 5. PID temperature control system PCB schematic diagram.

The MAX6675 digital thermometer module converts the thermocouple output signal into a 12-bit Analog to Digital Converter (ADC) number and sends it to the microcontroller via Serial Peripheral

Interface (SPI) communication. The Arduino Nano converts the ADC number into temperature in °C and sends it to a LabVIEW PID control program as a Process Variable (PV). As a response, the microcontroller receives Manipulated Variable (MV), a Pulse Width Modulation (PWM) signal duty cycle from the LabVIEW program. The corresponding PWM signal is generated by the microcontroller and received by the input pins of the SSR 40-DA to power the band heater.

Before using the temperature control system in the experimental procedures, we calibrated the temperature measurement system. An APPA51 digital thermometer module is connected to a type-K thermocouple identical to the one we used in the temperature control system. By assuming the APPA51 temperature readings as reference values, we generated an ADC to temperature conversion function of the MAX6675 module. After implementing the conversion function to the Arduino Nano, the temperature control system is ready to be used.

3. RESULTS AND DISCUSSION

In this part, we present the experimental results of the tests applied to the measurement system. The purposes of these tests are to obtain the system's performance qualities and determine its reliability when measuring the damping coefficient of a specific liquid sample.

3.1. Shaft Encoder Functionality Test

An ideal LPD3806-600BM-G5-24C shaft encoder generates 600 digital pulses per shaft rotation, so we decided to put it to the test [21]. The encoder shaft was rotated 20 times in both clockwise and counter-clockwise directions. We plotted the number of encoder output pulses against the number of shaft rotations and drew a linear regression line. The slope is the experimental number of pulses per shaft rotation. Fig.6 shows the test results.

The clockwise rotations resulted in approximately 597 pulses per shaft rotation, while the counter-clockwise' resulted in approximately 603 pulses per rotation. These values agree with the encoder's output specification, which is 600 pulses per shaft rotation. Suppose the encoder output signals are fed to the XOR gate input pins, as shown in the block diagram in Fig.2. In that case, the output will be a square wave signal with a frequency twice its inputs (approximately 1200 pulses per encoder shaft rotations).

In this test, the encoder shaft is manually rotated by hand for each rotation direction. Since random error occurs due to the motion of the hand, the number of output pulses differs in every rotation. Using the experimental values obtained in this test, we noticed that the total difference in the number of pulses between the two shaft rotational directions is 120. This number is much smaller than the total number of pulses generated by an ideal encoder, which is 12000 for twenty shaft rotations. This fact causes a similar look between graphs (a) and (b) in Fig.6.

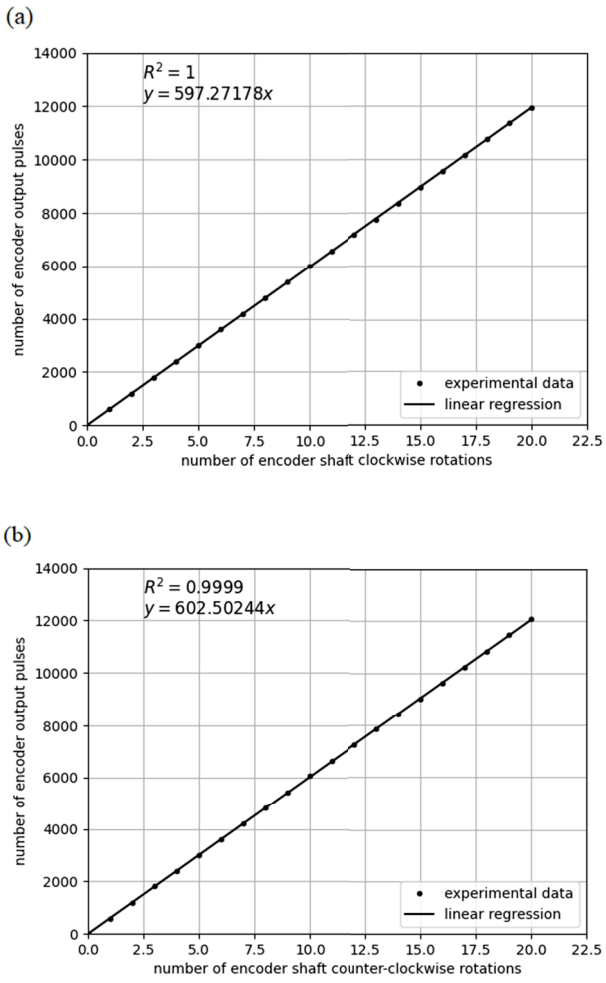

Figure 6. Shaft encoder output pulses: (a) Clockwise rotations; (b) Counter-clockwise rotations.

3.2. Band Heater Process Identification

The process model and the appropriate PID constants are obtained from identifying the band heater process. We heated an ISO VG 100 industrial oil sample and recorded PV versus time to identify the band heater process. This liquid sample is the one that will be used in the viscous damping coefficient measurement procedure. Fig.7 shows the experimental data, where the dashed line represents the duty cycle of the PWM signal, which is the Manipulated Variable of the process.

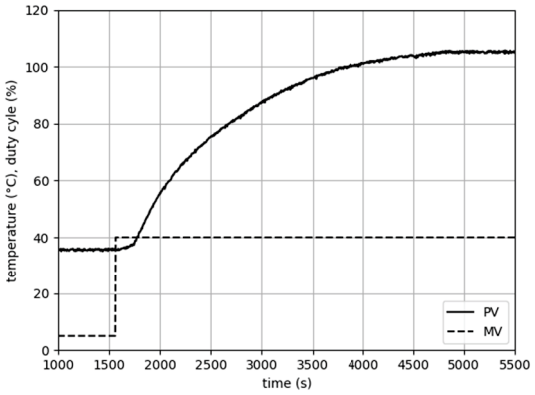

Figure 7. Band heater process curve.

The *First Order Plus Time Delay* (FOPTD) process model and the PID constants obtained from the process identification can be seen in Table.1, where the dimensionless controller gain is the integral time in seconds and is the derivative time in seconds. We used the Direct Synthesis method with Pade˜ approximation to calculate the three PID constants [22].

TABLE 1. Band heater PID controller settings.

No	$G_p(s)$	$\frac{1.99e^{-155s}}{960s+1}$
1	K_c	0.485
2	τ_I	1038
3	τ_D	71.7

3.3. PID Temperature Control

As reflected in Table.1, the PID temperature controller has a parallel form of the transfer function that can be written as in Eq. 3.

$$G_c(s) = 0.485\left(1 + \frac{1}{1038s} + 71.7s\right) \qquad (3)$$

To test the reliability of the PID temperature controller in a wide range of liquids, we applied the PID settings to heat six industrial oil samples until each one of them reached a steady temperature of 40 °C, even though the heating system could reach higher temperature points. To avoid overshoots, we chose a desired time constant value of 1000 s, which is larger than the process time constant, which has a value of 960 s. Fig.8 shows the results of the temperature controls.

We chose the temperature point of 40 °C as the *Set Point* (SP) of the PID control, because the reference viscosities of the *ISO VG* industrial oil samples are reported at this temperature value. The PV curves of the six liquid samples suggest that the PID temperature control system has succeeded in maintaining all sample temperatures at the desired value (40 °C). This fact encourages us to use the heater system for damping coefficient measurements.

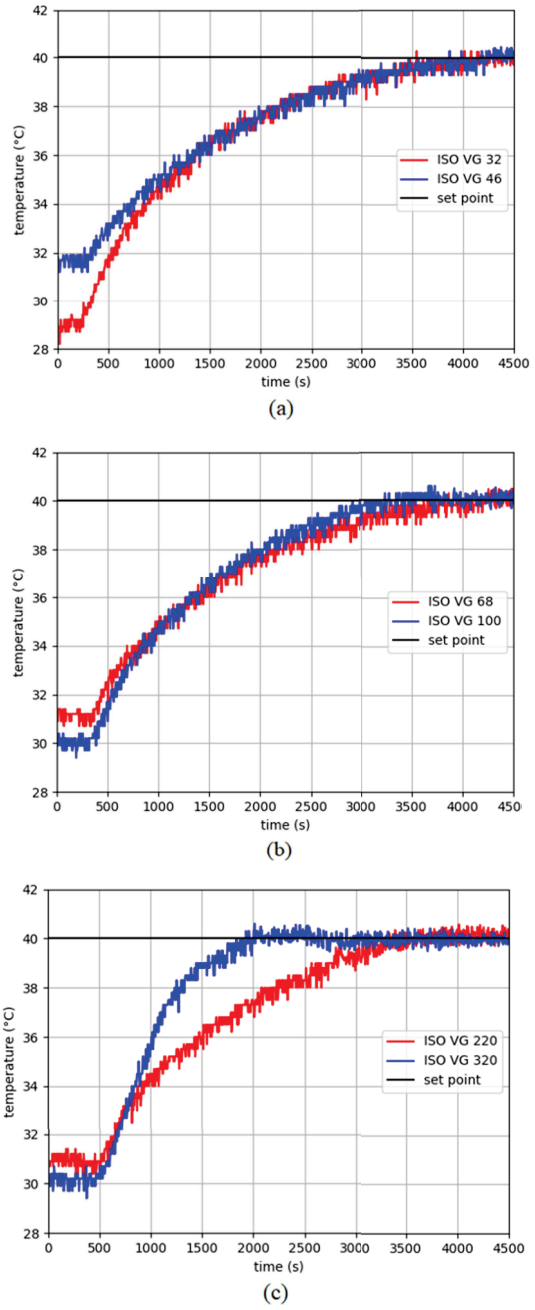

Figure 8. Sample temperature control results: (a) ISO VG 32 and ISO VG 46; (b) ISO VG 68 and ISO VG 100; (c) ISO VG 220 and ISO VG 320.

3.4. Damped Harmonic Oscillator Test

An oscillation test must be done before measuring the liquid damping coefficient without involving any liquid sample. The test results may help when observing the data acquisition system's performance and analyzing the damping effect due

to the air resistance and friction of the mechanical components. Fig.9 shows one of ten repetition test results of the damped harmonic oscillator, where is the first amplitude, is the damping coefficient, is time, and is the total mass of the system where.

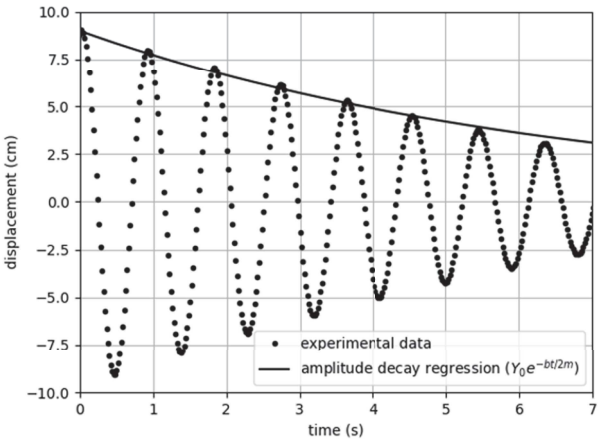

Figure 9. Damped harmonic oscillator test result.

The air resistance and the total friction of the bearings (including the shaft encoders) create a significant decrease in the oscillation amplitude. This statement is based on the average damping coefficient obtained from ten repetition measurements with a value of. An ideal harmonic oscillator system should have zero damping coefficient, meaning there are no air resistance and mechanical friction, which dampens the oscillation.

3.5. Measurement Repeatability Test

A repeatability test measured the damping coefficient of the prolate ellipsoid's underdamped oscillatory motion underneath a viscous liquid. Since we are focusing only on the system's precision when measuring a sample multiple times, we decided to use only one sample, the ISO VG 100 oil. The sample was tested ten times at a constant temperature of 40 °C. Fig.10 shows the experimental results of the ten damping coefficient measurement repetitions.

The repeatability test of the measurement system gave us a decent result. This statement is supported by the fact that the ten repetitional damping coefficient data has a 1.3% of *relative standard deviation* (RSD). This repeatability RSD value is small enough for a measurement system that is manually made from scratch. We are aware that we want to create a fully functional viscometer in future studies; some derivations will be needed to obtain the suitable expression of dynamic viscosity as a function of the viscous damping coefficient.

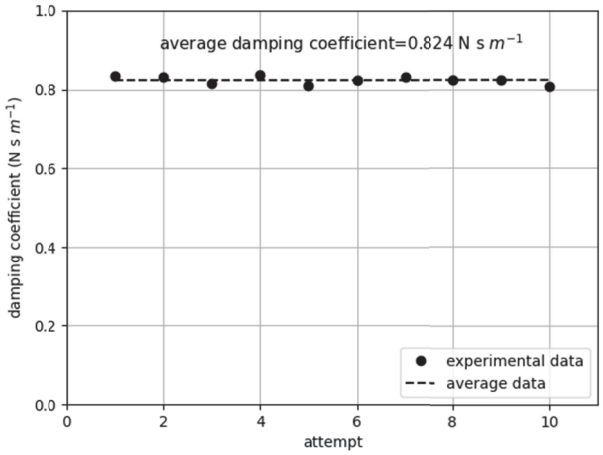

Figure 10. Measurement repeatability test result.

4. CONCLUSION

We have built and tested a damping coefficient measurement system based on an underdamped harmonic oscillator. We used an incremental optical encoder as the motion detector because it can convert the angular shaft position and rotation direction into a pair of square wave signals. The data acquisition system records and visualize the prolate ellipsoid's displacement against time during the oscillatory motion. A PID-based temperature control system was added to maintain the sample's temperature during the measurement. Finally, a repeatability test of the measurement system using an ISO VG 100 oil sample resulted in a 1.3% of relative standard deviation. In order to create a fully functional viscometer in future studies, some derivations will be needed to obtain the suitable expression of dynamic viscosity as a function of the viscous damping coefficient.

5. ACKNOWLEDGMENTS

The authors thank the Department of Physics, Faculty of Mathematics and Natural Sciences, Universitas Indonesia, for providing the research facilities.

REFERENCES

1. Li D, Kong N, Zhang B, Zhang B, Li R, Zhang Q. Comparative study on the effects of oil viscosity on typical coatings for automotive engine components under simulated lubrication conditions. Diam Relat Mater [Internet]. 2020;108226. Available from: https://doi.org/10.1016/j.diamond.2020.108226
2. Sukkar KA, Karamalluh A, Aber TN. Rheological and Thermal Properties of Lubricating Oil Enhanced by the Effect of CuO and TiO2 Nano-Additives. Al-Khwarizmi Eng J. 2019;15(2):24–33.
3. Štěpina V, Veselý V. Tribology series, 23, LUBRICANTS AND SPECIAL FLUIDS. Czecho-Slovakia: Elsevier Science Publishers; 1992.

4. Špeťuch1 V, Petrík J, Grambálová E, Medveď D, Palfy P. The Capability of The Viscosity Measurement Process. Acta Metall Slovaca. 2015;21(1):53–60.

5. Barnes HA. An examination of the use of rotational viscometers for the quality control of non-Newtonian liquid products in factories Howard. Appl Rheol. 2001;11(2):89–101.

6. Aruna S, Shantha G. Analysis On Different Types of Viscometers, Design, Materials and Technology. Turkish J Comput Math Educ. 2020;11(3):978–82.

7. Bridges S, Robinson L. A Practical Handbook for Drilling Fluids. Gulf Professional Publishing is an imprint of Elsevier; 2020.

8. ÇENGEL YA, CIMBALA JM. Fluid mechanics. 1st ed. McGraw-Hill series in mechanical engineering; 2006.

9. King GC. Vibrations And Waves. LOEBINGER FK, MANDL F, SANDIFORD DJ, editors. United Kingdom: A John Wiley and Sons, Ltd., Publication; 2009.

10. Alexander P, Indelicato E. A semiempirical approach to a viscously damped oscillating sphere. Eur J Phys [Internet]. 2005;26(August):1–10. Available from: stacks.iop.org/EJP/26/1

11. Shamim S, Zia W, Anwar MS, Shamim S, Zia W, Sabieh M. Investigating viscous damping using a webcam. Am Assoc Phys Teach. 2010;78(4).

12. JE Escalante-Martı nez, ´mez-Aguilar JG, ´n CC´-R, Morales-Mendoza L, ˜a IC-O, Laguna-Camacho J. Experimental evaluation of viscous damping coefficient in the fractional underdamped oscillator. Adv Mech Eng. 2016;8(4):1–12.

13. Roy S kumar, Mohanty AR. Use of rotary optical encoder for firing detection in a spark ignition engine. Measurement [Internet]. 2017;98:60–7. Available from: http://dx.doi.org/10.1016/j.measurement.2016.11.026

14. Kadhum AA, Abdulhussein MM. Implementation dc motor as servomotor by using arduino and optical rotary encoder. In: Sakthivel S, Karthikeyan S, Palani IA, editors. Materials Today: Proceedings [Internet]. Elsevier Ltd; 2021. p. 4–8. Available from: https://doi.org/10.1016/j.matpr.2021.03.576

15. Ike E. The Study of Viscosity-Temperature Dependence and Activation Energy for Palm Oil and Soybean Oil. Glob J PURE Appl Sci. 2019;25:209–17.

16. Gunawan O, Virgus Y. The one-dimensional camelback potential in the parallel dipole line trap: Stability conditions and finite size effect. J Appl Physics121 [Internet]. 2017;121(November 2011). Available from: http://dx.doi.org/10.1063/1.4978876

17. Happel J, Brenner H. Low Reynolds number hydrodynamics with special applications to particulate media. MARTINUS NIJHOFF PUBLISHERS k; 1983. 4-7 p.

18. Chowdary GR, Krishna TVR, Pavan MS, Mahesh MUV, Tejaswi P. Design and Performance Evaluation of D-Flip-Flop using Various Technology Nodes. 2020;8(5):13–8.

19. M B, A SKG. In-Depth Survey on XOR Gate Design. J Crit Rev. 2020;7(18).

20. Chevron Marine Products LLC. viscosity classifications. Mar Lubr Inf Bull 6. 2019;

21. Oguntosin V, Akindele A. Design of a joint angle measurement system for the rotary joint of a robotic arm using an Incremental Rotary Encoder. J Phys Conf Ser. 2019;1299(1).

22. Seborg DE, Edgar TF, Mellichamp DA, III FJD. Scilab Textbook Companion for Process Dynamics And Controls Book Description. 3rd ed. John Wiley And Sons (Asia) Pvt. Ltd.; 2013. 211-230 p.